Point spread function reconstruction for Single-conjugate Adaptive Optics on Extremely Large Telescopes

Roland Wagner*, Christoph Hofer†, Ronny Ramlau‡

August 28, 2018

Abstract

Modern ground-based telescopes like the planned Extremely Large Telescope (ELT) depend heavily on Adaptive Optics (AO) systems to correct for atmospheric turbulence. Even though AO correction is used, the quality of astronomical images still is degraded due to the time delay stemming from the wavefront sensor (WFS) integration time and temporal response of the deformable mirror(s) (DM). This results in a blur which can be mathematically described by a convolution of the true image with the point spread function (PSF).

In this paper, we present an algorithm for SCAO PSF reconstruction adapted to the needs of ELTs in a storage efficient way. In particular, the classical PSF reconstruction algorithm from [34] is changed in several points to give a more accurate estimate for the post-AO PSF. Bilinear splines are used as basis functions in order to minimize the computational effort.

Results obtained in an end-to-end simulation tool show qualitatively good reconstruction of the PSF compared to the PSF calculated directly from the simulated incoming wavefront. Furthermore, the used algorithm has a reasonable runtime and memory consumption.

---

*Industrial Mathematics Institute, Johannes Kepler University, Linz, Austria. wagner@indmath.uni-linz.ac.at

†Doctoral Program Computational Mathematics, JKU Linz, Austria

‡Industrial Mathematics Institute, JKU Linz and Johann Radon Institute for Computational and Applied Mathematics (RICAM), Linz, Austria

1 Introduction

In ground-based astronomy, the observed image I_o can be described as a convolution of the true image I and the so-called point spread function (PSF), i.e.,

$$I_o = I * \mathcal{PSF}.$$

The PSF of an astronomical observation through a ground-based telescope depends on the one hand on the geometry of the telescope and the atmospheric turbulence above the telescope and on the other hand on the design of the used instrument including its technical specification, in particular regarding static aberrations. Modern ground-based telescopes reduce the effect of the turbulent atmosphere by Adaptive Optics (AO) systems. However, still residual turbulences remain uncorrected. The goal is to reconstruct the PSF from data acquired by the wavefront sensors (WFS) and the commands applied to the deformable mirror(s) (DM) after the image has been obtained. This task is required as part of operating the upcoming extremely large telescopes (ELTs), such as the European ELT [15] and its first light instruments MICADO [11] and METIS [5]. Availabilitiy of the PSF allows to access parameters which determine the quality of an observation, without estimating them from the science image and gives information on the blurring effect coming from atmospheric turbulence and the telescope optics. Additionally, the PSF can be used for image improvement in a post processing step, such as deconvolution (see, e.g., [14, 9, 12, 13, 28]).

The purpose of this paper is to describe an algorithm for PSF reconstruction in Single-Conjugate Adaptive Optics (SCAO), starting from a purely mathematical formulation and trying to do as little simplifications as possible to obtain high accuracy, while at the same time making a trade-off to keep the computational costs reasonable. In a post-processing step, the quality of AO-corrected images can be further improved by using deconvolution algorithms where the knowledge of the PSF is required. Furthermore, the PSF can be used to extract estimates for parameters such as Strehl ratio or Encircled Energy.

PSF reconstruction is based on the WFS data, which is acquired at a frequency of 500 to 3000 Hz, under excellent seeing conditions even frame rates of 100 Hz or lower might be used. Saving the measured data and performing calculations in a post-processing step will result in an enormous amount of data as the image exposure time ranges from one second to several minutes. Note that we consider only the reconstruction of the PSF in the direction of

the guide star (on-axis). For a field of view (FoV) larger than around 10",
knowledge of the PSF in different directions is required, as then the PSF is
spatially varying within the FoV due to so-called anisoplanatism [18]. Even
in the narrow field case, the PSF might vary due to field-dependent static
aberrations of the science instrument which remain uncorrected after apply-
ing methods such as in [1, 33, 30].

One major drawback of the upcoming ELTs, such as the European ELT,
and the corresponding instruments is the relatively coarse resolution of the
WFS, roughly 0.5 m subaperture size projected onto the primary mirror.
This results in a large part of unknown higher order terms of the wavefront.
Such a coarse resolution of the WFS becomes necessary due to the faint stars
serving as guide stars (GS). Choosing a higher resolution of the WFS would
result in having a too low signal to noise ratio in the WFS measurements.
This influences also the actuator spacing of the DM, which will be roughly
of the same size. However, a bigger size of the primary mirror still leads to
a quadratic increase in the degrees of freedom to adjust the DM and thus
much more data which has to be handled on the fly and/or stored for post-
processing.

We propose an algorithm for SCAO PSF reconstruction adapted to the
needs of ELTs in a storage efficient way. In particular, we adopt the classical
PSF reconstruction algorithm from [34], by using a 4D structure function in-
stead of a 2D structure function as well as very local basis functions [21, 35].
In particular, we do not compute covariance matrices from WFS data rather
than from applied DM updates, resulting in a method dependent on the WFS
type and AO control algorithm only in noise and aliasing propagation. This
eases the use of PSF reconstruction as the decision on the WFS sensor type
is still under discussion for METIS and MICADO and we want our algorithm
to be usable with upcoming Pyramid WFS as well. In our approach, we use
a method with linear complexity to get from WFS data to wavefronts, the
so-called CuReD method, see [37, 31, 32], instead of the classical Matrix-
approach which results in quadratic complexity. The use of linear methods
for wavefront reconstruction is under investigation within the ELT instru-
ment consortia as ELTs require faster methods than existing telescopes and
therefore CuReD is a good choice. All proposed steps are done for closed-
loop AO systems.

In the following Section, we recall the original algorithm from [34] and
highlight some of its limits for reconstructing the PSF from WFS data. We
present our new approach in Section 3. Section 4 shows results obtained with

ESO's end-to-end simulation tool Octopus.

2   PSF reconstruction for SCAO

In order to have a good understanding of existing algorithms, we give a short review of Véran's algorithm, first presented in [34].

The following assumptions were in [34]: First, the corrected phase at any position on the pupil has a Gaussian statistics and the integration time is long enough so that the statistical average can be substituted by the temporal average. Second, the structure function of the residual phase, defined as

$$D_\phi(\mathbf{x}, \boldsymbol{\rho}) = \langle |\phi(\mathbf{x}, t) - \phi(\mathbf{x} + \boldsymbol{\rho}, t)|^2 \rangle_t,$$

with $\langle \cdot \rangle_t$ the temporal average of a function, is replaced by its spatial average. Third, the residual incoming phase ϕ is split into a component in the space spanned by the mirror modes $\phi_\parallel$ and into a higher order component $\phi_\perp$, i.e., $\phi = \phi_\parallel + \phi_\perp$. This results in a formula for the long exposure optical transfer function (OTF) in the near field approximation for a monochromatic image at wavelength λ as in [34]:

$$B(\boldsymbol{\rho}/\lambda) = \underbrace{\exp\left(-\frac{1}{2}\bar{D}_{\phi_\parallel}(\boldsymbol{\rho})\right)}_{B_\parallel(\boldsymbol{\rho}/\lambda)} \underbrace{\exp\left(-\frac{1}{2}\bar{D}_{\phi_\perp}(\boldsymbol{\rho})\right)}_{B_\perp(\boldsymbol{\rho}/\lambda)} \underbrace{\int_{\mathcal{P}} P(\mathbf{x})P(\mathbf{x}+\boldsymbol{\rho})d\mathbf{x}}_{B_{tel}(\boldsymbol{\rho}/\lambda)}. \quad (1)$$

The terms $\bar{D}_{\phi_\parallel}$ and $\bar{D}_{\phi_\perp}$ represent the spatial averaged structure functions of $\phi_\perp$ and $\phi_\parallel$, respectively. Crossterms between these two parts drop off, if the space of mirror modes is perpendicular to the space of higher order components. Note that in numerical computations this corresponds to a good choice of basis functions. Using Zernike polynomials as ansatz functions as done in [34] will introduce non-zero crossterms as these do not form a basis on the ELT aperture.

The three parts of (1) can be reconstructed separately: $B_\parallel$ can be estimated from control loop AO data in the on-axis case, $B_\perp$ can be estimated from simulated data only and B_{tel} is given analytically. The first two terms clearly depend on the seeing conditions of the current observation. Therefore an algorithm to estimate the seeing from AO loop data was developed. The quantity $B_\perp$ has to be simulated only once and can then be scaled to the current observing conditions. Note that we do not consider the off-axis case and, therefore, the dependence of $B_\parallel$ on the atmospheric conditions is not

discussed.

To be able to compute $\bar{D}_{\phi_\parallel}(\boldsymbol{\rho})$ fast, Véran introduced functions $U_{ij}(\boldsymbol{\rho})$ that depend on the possible mirror modes and can be precomputed numerically. For the remaining calculations, only the time-averaged covariances of the WFS data are needed. As the original algorithm was proposed for Zernike polynomials, this method turned out to give good results, but still was time and memory consuming. Therefore, [19] diagonalized Véran's approach using so-called V_{ii}-functions, where an eigenvalue decomposition of the computed covariance matrix is needed, which gives a speedup for certain basis functions. With the increasing telescope size and changes in the telescope geometry, e.g., due to spiders, Zernike polynomials do not seem feasible as they form no basis, but still have global support.

For the computation of $\bar{D}_{\phi_\perp}(\boldsymbol{\rho})$, a Monte Carlo method is proposed, where the high order components of randomly generated phase screens with Kolmogorov or Von Kármán statistics are extracted and then using a temporal and spatial average for the structure function.

In terms of the resolution, the accuracy of PSF reconstruction is limited by the hardware of the telescope, e.g., the physical setup of the used DM, i.e., the spacing between the actuators. This resolution is rather coarse and limits the part of $\phi_\parallel$ to the DM cut off frequency, resulting in a rather coarse estimate for the structure function.

The applied DM shapes being derived from WFS measurements suffer from imperfections of these devices as it holds that an aliasing error occurs, i.e., $\Gamma\phi_\perp \neq 0$, where Γ is the Shack-Hartmann WFS operator, that maps incoming wavefronts to measurements. This influences the reconstructed wavefronts and/or atmospheric layers and, as a result, changes $D_{\phi_\parallel}$ slightly. In addition to that, there is some measurement noise in $\Gamma\phi$, leading to further changes in the structure function. The latter one can be modeled and thus corrected if one has a good knowledge of the WFS. For good estimates of $D_{\phi_\perp}$, the seeing parameter r_0 (or D/r_0) is needed for the calculation of $\phi_\perp$ and for estimating the influence of $\Gamma\phi_\perp$ on the PSF. A good estimate can be obtained by using, e.g., the iterative procedure from [34].

When going on sky with a PSF reconstruction algorithm, one has to adjust for non common path aberrations, as the optical path to the WFS and the science camera are not the same. In the algorithm above this means that B_{tel} is not only calculated from the pupil function but can be calibrated

in form of a static PSF as the non common path aberrations (NCPA) are static. Note that the adjustments necessary to compensate for this effect can be obtained via calibration as the non common path aberrations are static at much longer time scales than atmospheric aberrations. However, one still has to obtain a good understanding of NCPAs to make use of the reconstruced PSFs for science. A discussion on characterizing and minimizing the impact of NCPAs can be found, e.g., in [29].

Since the proposal of Véran's algorithm in [34], computational power and available memory increased, therefore some adjustments of the algorithm to improve the quality are possible in feasible computational time. In particular, it was never demonstrated that Zernike polynomials as basis functions are an appropriate choice for modern deformable mirrors with completely different influence functions. Furthermore, the required computational power for Zernike polynomials is rather high due to their global support, which results in full and dense matrices. We want to use basis functions with local support in order to reduce the computational complexity and to be able to account for the four-dimensionality of the structure function, which was demonstrated to be possible already in [20]. The 2D calcuation in [34] is one of the limitations as it reduces the accuracy and needs the assumption of a stationary residual phase. However, on ELT-size the residual phase might be non-stationary anymore due to the changed characteristic sizes. Note that using four-dimensional functions might not be critical in terms of accuracy, but still a more accurate model of the reality and computationally feasible.

Note that aside from Véran's approach also other methods were proposed, e.g., in [16], which takes a maximum likelihood approach for the used covariance matrices, or [26], where only open loop data is taken into account and a fine resolution WF is created by combining measurements from different timesteps. Some of the algorithms were already successfully tested on sky on various telescopes [23, 22, 17, 8, 25]. Algorithms for on-axis PSF reconstruction in SCAO suffer from anisoplanatism, when used to estimate off-axis PSFs. An approach to overcome these difficulties has been presented in [6, 2]. It can be combined with our algorithm in order to obtain PSFs for each point in the field of view. In [7] an $\ell^1 - \ell^2$ model for PSF reconstruction is proposed to create high-resolution phase gradients from subsequent WFS frames and obtain an estimate of the instantaneous PSF when no AO correction is used. As pointed out in [10], prior to the reconstruction algorithms the PSF of a reference star was measured from a separate observation directly before or after the science observation and then used for deconvolution algorithms (see, e.g., [14, 9, 12, 13, 28] and references therein). However, this approach

implicitly uses the strong assumptions that the atmospheric conditions are sufficiently stable and that the flux and intensity on the WFS are the same for the PSF reference star and the target's guide star.

3 Novel approach to PSF reconstruction for SCAO

3.1 Updating PSF reconstruction for SCAO

We start from the long exposure OTF, i.e.,

$$B(\boldsymbol{\rho}/\lambda) = \frac{1}{S} \int_{\mathbb{R}^2} P(\mathbf{x}) P(\mathbf{x} + \boldsymbol{\rho}) e^{-\frac{1}{2} D_\phi(\mathbf{x}, \boldsymbol{\rho})} \, d\mathbf{x}, \tag{2}$$

where $D_\phi(\mathbf{x}, \boldsymbol{\rho}) = \langle |\phi(\mathbf{x}, t) - \phi(\mathbf{x} + \boldsymbol{\rho}, t)|^2 \rangle$, and make some adjustments. The exact calculation of $B(\boldsymbol{\rho}/\lambda)$ requires averaging four-dimensional functions, which seemed computationally too demanding when Véran developed his algorithm and thus proposed to interchange spatial average and the exponential function to overcome this problem. Nowadays this simplification can be partly dropped, as these computations are possible in reasonable time even on a laptop as shown, e.g., in [17, 20].

As a starting point of our approach, we split ϕ into a part seen by the WFS (and thus corrected by the DM in the following time step), called $\phi_\parallel$, and a part orthogonal to the DM modes, called $\phi_\perp$. Clearly, $\phi = \phi_\parallel + \phi_\perp$ and thus

$$D_\phi(\mathbf{x}, \boldsymbol{\rho}) = D_{\phi_\parallel}(\mathbf{x}, \boldsymbol{\rho}) + D_{\phi_\perp}(\mathbf{x}, \boldsymbol{\rho})$$
$$+ 2\langle [\phi_\parallel(\mathbf{x}, t) - \phi_\parallel(\mathbf{x} + \boldsymbol{\rho}, t)][\phi_\perp(\mathbf{x}, t) - \phi_\perp(\mathbf{x} + \boldsymbol{\rho}, t)] \rangle_t.$$

Note that in [34] this splitting was made after interchanging spatial average and the exponential.

The last term is a cross term between differences of two orthogonal terms and is zero, when choosing basis functions as ansatz functions for numerical computations. Thus, the OTF can be rewritten as

$$B(\boldsymbol{\rho}/\lambda) = \frac{1}{S} \int_{\mathcal{P}} P(\mathbf{x}) P(\mathbf{x} + \boldsymbol{\rho}) \exp\left(-\frac{1}{2} D_{\phi_\parallel}(\mathbf{x}, \boldsymbol{\rho})\right)$$
$$\times \exp\left(-\frac{1}{2} D_{\phi_\perp}(\mathbf{x}, \boldsymbol{\rho})\right) d\mathbf{x}.$$

The orthogonal part of the residual phase cannot be obtained from the actual on sky data as it is not represented on the DM, but only simulated offline by using sophisticated atmospheric models. Therefore, using one realization of $\phi_\perp$ for the calculation of $D_{\phi_\perp}(\mathbf{x}, \boldsymbol{\rho})$ gives no meaningful contribution and we follow partly the suggestion of [34] to replace it by $\bar{D}_{\phi_\perp}(\boldsymbol{\rho})$, its mean over the variable $\mathbf{x}$ given by

$$\bar{D}_{\phi_\perp}(\boldsymbol{\rho}) = \frac{\int_\mathcal{P} P(\mathbf{x})P(\mathbf{x} + \boldsymbol{\rho})D_{\phi_\perp}(\mathbf{x}, \boldsymbol{\rho})d\mathbf{x}}{\int_\mathcal{P} P(\mathbf{x})P(\mathbf{x} + \boldsymbol{\rho})d\mathbf{x}}.$$

Note that this is equivalent to assuming a small enough dispersion in $\mathbf{x}$, which is still valid as the higher order component $\phi_\perp$ is only a part of ϕ. Hence, (2) simplifies to

$$B(\boldsymbol{\rho}/\lambda) = \frac{1}{S}\exp\left(-\frac{1}{2}\bar{D}_{\phi_\perp}(\boldsymbol{\rho})\right)$$
$$\times \int_\mathcal{P} P(\mathbf{x})P(\mathbf{x} + \boldsymbol{\rho})\exp\left(-\frac{1}{2}D_{\phi_\parallel}(\mathbf{x}, \boldsymbol{\rho})\right)d\mathbf{x},$$

which is a product of two independent terms. The first term can be estimated only from simulation, as $\phi_\perp$ is not available on sky, while the second term has to be calculated on the fly from closed loop AO measurements using $\phi_\parallel$. Note that, when using the original method from [34], also the structure function of $\phi_\parallel$ is averaged over $\mathbf{x}$, which results in three independent components: the OTF of the telescope in absence of turbulence, the contribution of the mirror component and the contribution of the higher order phase. In our approach, however, the first two components are combined into one.

3.2   Changing the basis functions

To implement the above ideas numerically, we need to choose basis functions that fit our needs. For an ELT, one would have to compute roughly 5000^2 of U_{ij}-functions when using the original Véran algorithm. With certain basis functions, these computations can be performed efficiently. For this purpose, basis functions with local support are clearly a good choice. In particular, if one considers the use of linear influence functions for future DMs, one could think of using, e.g., bilinear splines as basis functions for the U_{ij}-algorithm as proposed in [21]. The bilinear splines $\varphi_{i,j}$ are defined by their values on the corners of the subapertures of an $n \times n$ Shack-Hartmann WFS, i.e., for the corner point of subaperture $(\bar{i}, \bar{j})$ with coordinates $(x_{\bar{i}}, y_{\bar{j}})$, it holds that

$$\varphi_{i,j}(x_{\bar{i}}, y_{\bar{j}}) = \delta_{i,\bar{i}}\delta_{j,\bar{j}}, \quad \forall i, j = 1, \ldots, n,$$

where $\delta_{k,l}$ denotes the usual Kronecker symbol, i.e., $\delta_{k,l} = 1$ for $k = l$ and 0 else. Due to this special choice, it holds that a wavefront $\overline{\varphi}$ in this basis takes the coefficient $c_{p,q}$ as value in the corresponding node with coordinates $(\bar{x}_p, \bar{y}_q)$, i.e.,

$$\overline{\varphi}(\bar{x}_p, \bar{y}_q) = c_{p,q}.$$

Computing the corresponding U_{ij}-functions on the same grid points results in just evaluating whether the two indices match or not. This change leads to a sparse representation of the needed matrices for the noise and aliasing part. However, it turns out that the U_{ij}-functions do not even have to be computed, but the corresponding structure functions can be computed directly when running Monte Carlo simulations for noise and aliasing. Furthermore, note that modern and future DMs will not have linear influence functions, but still bilinear splines are a good first order approximation of the influence functions. This approach can be performed for any kind of local functions, thus also for influence functions of modern DMs. However, in this case the computational cost will increase.

Clearly, the higher order parts of the wavefront cannot be represented on this grid, but we use a finer grid to compute the corresponding structure function. Note that the resolution of $\phi_\perp$ corresponds to how far out the PSF should be reconstructed. Numerical experiments showed that taking a resolution four times finer than the DM provides a good reconstruction of the PSF for a radius of almost 2000 mas. However, the computations on such a resolution require a bigger memory and more operations. Since the higher order components $\phi_\perp$ are precomputed and appropriately scaled to current observation conditions, this is not a crucial issue with modern computers.

Note that we do not use the V_{ii}-algorithm as these functions have to be calculated on the fly and therefore lead to an increased computation time for the structure function in our setting, as demonstrated in [21].

3.3   Using wavefronts instead of WFS measurements

In the original algorithm from [34], the WFS measurements were used as a starting point and all calculations were based directly on the WFS measurements. However, the structure function of an AO run, D_ϕ, is directly related to the incoming wavefronts. As the incoming wavefronts are reconstructed to obtain the shape of the DM, we propose to use these reconstructions directly for the estimation of D_ϕ. Note that the reconstructed incoming wavefront ϕ_{rec} is only an estimate for the true parallel phase $\phi_\parallel$. Assuming

that $\phi_{rec} = \phi_{\parallel} + \phi_n + \phi_r$, where ϕ_n is the WFS noise propagated into DM commands and ϕ_r is the higher order component giving a non-zero measurement and being propagated into DM commands, i.e. $\phi_r = R\Gamma\phi_{\perp}$, with Γ the SH-WFS operator and R the AO control algorithm. We need to model the structure functions for noise ϕ_n and aliasing ϕ_r separately. This results in a splitting of the structure function for the parallel part, using the same ideas as [34] and assuming that noise and aliasing are independent and stationary leaves us with three terms:

$$D_{\phi_{\parallel}}(\mathbf{x}, \boldsymbol{\rho}) \approx D_{\phi_{rec}}(\mathbf{x}, \boldsymbol{\rho}) - \bar{D}_{\phi_n}(\boldsymbol{\rho}) + \bar{D}_{\phi_r}(\boldsymbol{\rho}). \tag{3}$$

Let us describe how the three terms of (3) can be computed. First, the structure function $D_{\phi_{rec}}$ relies on the applied DM commands. For an SCAO system, commonly matrix-vector-multiplication (MVM) is used for the reconstruction process. Recently, matrix-free algorithms, such as CuReD [37, 31, 32], HWR [3], both tested on sky [4], and FinECuReD [27, 36], were introduced. Thus, starting from reconstructed wavefronts instead of WFS measurements does not increase the computational complexity. Certain effects such as sensor noise still have to be modeled on measurement level and then transferred onto the wavefront level, but these are computations which can be done prior to the AO and PSF reconstruction run and therefore have no effect on the runtime.

In [34] the command matrix is used to obtain a covariance matrix, which is $\mathcal{O}(N^2)$ for N subapertures on the WFS. In our approach, we do not go directly from measurements to the covariance matrix, as we use a matrix-free AO control algorithm (CuReD), being only $\mathcal{O}(N)$, where setting up the matrix would use more computational power than actually needed. Therefore, we split this into two parts: First from WFS data we reconstruct the incoming wavefront on our bilinear spline basis ϕ_{rec}, second we compute from this wavefront the structure function $D_{\phi_{rec}}$. This approach benefits from the fact that during AO run the AO control algorithm has to be stable, so it might not be the best possible reconstruction, in a sense that the parameters of the AO control algorithm will be fixed for one observation in order to meet run time and quality requirements. However, one might think of recomputing the DM updates from the WFS frames by using a different control algorithm, which needs parameter tuning and/or longer run time, but provides superior reconstruction quality. In our two step approach, we can fine tune the reconstruction method for one specific observation, using, e.g., additionally available information on seeing and atmospheric conditions. Furthermore, it is easy to adapt this approach for other WFS as, e.g., MICADO and METIS

show tendencies to use Pyramid WFS for the SCAO modules. The only modification needed is thus to replace the reconstruction method and while the other components of the algorithm do not change.

The structure functions for noise and aliasing $\bar{D}_{\phi_n}$ and $\bar{D}_{\phi_r}$ are spatially averaged, which we get by using Monte Carlo simulations to obtain realizations of ϕ_n and ϕ_r and computing these structure functions directly. We assume a Gaussian white noise covariance matrix on the wavefront sensor $C_{WFS} = \frac{1}{n_{photons}}I$. To obtain ϕ_r, we simulate $\phi_\perp$, compute the respective SH measurements $\Gamma\phi_\perp$ and use CuReD as AO control algorithm. Furthermore, note that the noise and aliasing structure functions are computed only once as a starting point and updates can be performed offline, so one could use available covariance matrices together with the U_{ij}-functions as proposed in [34]. However, when using a matrix-free AO control algorithm this would mean that one needs to set up the matrix which can easily be done by computing the response of the algorithm to only one non-zero measurement.

4   Numerical results

In this section, we present some further details on the estimation of the structure function of the higher order components of the incoming phase $\bar{D}_{\phi_\perp}$. Furthermore, results for PSF reconstruction in an SCAO system are shown for different guide star flux.

Note that we are not providing a direct comparison to the original Véran algorithm for the following reason. We tried two implementations for our algorithm: The first implementation evaluating the U_{ij}-functions based on bilinear splines which results in a huge computational effort even though only few integrals have to be evaluated. For the second implementation, we exploited the locality of the basis functions analytically and thus implemented only the necessary operations for points where the U_{ij}-functions are non-zero, giving a matrix-free method. This change in implementation resulted in avoiding the calculation and storage of all U_{ij}-functions. Additionally, we expect that when calculating U_{ij}-functions from a Zernike basis we cannot be sure that we took the same implementation as the authors of the original work. Furthermore, we would need a tuned ELT-size MVM to map from WFS data to incoming wavefronts. Note, that the original work was presented for a curvature WFS but was already adapted to Shack-Hartmann WFS (see, e.g., [23]).

4.1 Setting for numerical simulations

To verify that the proposed algorithm works well, we tested it in ESO's end-to-end simulation tool OCTOPUS for a planned ELT SCAO setting using WFS data from one NGS as described in Table 1. The decision for using OCTOPUS is based on the fact that it can directly provide the PSF corresponding to an AO loop for specified directions.

To get a better view on the effects of guide stars with different brightness on the PSF, the tests are performed for different photon flux from the NGS, but during one test run the flux is fixed. The photon flux varies for all tests between 100 and 1000 photons/subaperture/time frame. We do consider only small noise coming from the detector readout and the incoming photons. Note that the WFS setting stems from a preliminary design for the METIS instrument at the ELT, but a similar setting is also planned for the MICADO instrument. For reconstructing the incoming wavefront, and thus controlling the DM, CuReD (cf, [37, 31]) is used. The atmosphere in our simulations is a proprietary ELT ESO atmosphere[24] with 10 layers and a seeing $r_0 = 12.1$ cm at 500 nm (see Table 2). We use this atmosphere as it was communicated as preliminary setting for our AO control tests and therefore we already had a good and stable AO control algorithm when starting this project.

Telescope diameter	37 m
central obstruction	10.36 m
1 NGS Shack-Hartmann WFS	74×74 subapertures
WFS wavelength λ	0.7 μm
WFS integration time	2 ms
DM actuator spacing d_{DM}	0.5 m
science wavelength λ	2.2 μm
Simulation time	4 s real time (2000 time steps)

Table 1: Description of the simulated SCAO system

4.2 High order components of the incoming phase

In order to reconstruct the PSF properly, we need to have an estimate for $\bar{D}_{\phi_\perp}$. This estimate can only be obtained by simulation, in our case using

Layer	1	2	3	4	5	6	7	8	9	10
Height (m)	123.8	251.4	415	740.9	1394	2699	5309	9079	12849	16329
c_n^2-profile	0.59	0.02	0.04	0.06	0.01	0.05	0.09	0.04	0.05	0.05
windspeed (m/s)	6.555	5.865	5.06	4.485	5.06	8.28	16.33	30.245	34.27	17.48

Table 2: 10-layer atmosphere

OCTOPUS. As a feature, OCTOPUS provides the possibility to save incoming phase screens ϕ and the residual screens after AO correction. Note that this is a different simulation run then the one used for performing the reconstruction of the PSF. Even for application to on-sky data, this simulation will always be necessary in order to estimate $\bar{D}_{\phi_\perp}$ for the atmospheric conditions of the observation.

We filter out the DM modes from the simulated incoming screens to extract the residual phase $\phi_\perp$ from ϕ and then downsample the residual phase to bigger pixel size as otherwise calculating the structure function would be computationally too heavy. In this downsampling procedure, the choice of the basis functions for numerical implementation plays a crucial role. If one wants to choose a basis built up by bilinear splines, calculating $\bar{D}_{\phi_\perp}$ on the same grid as the DM updates (and WFS measurements) will not be successful. The main reason for this is that a DM with linear influence functions is able to perfectly correct for bilinear splines. Thus a finer grid for the calculation of $\phi_{\perp,n}$, and therefore $\bar{D}_{\phi_\perp}$ is needed. Results are provided for pixel size $\delta x = \frac{1}{4} d_{DM} = 0.125\ m$, as $d_{DM} = 0.5\ m$ is the spacing of the DM actuators in our simulations, and also the size of one WFS subaperture.

Additionally, in order to avoid temporal correlation in $\bar{D}_{\phi_\perp}$, we perform the temporal average not over every $\phi_\perp$ but take only every 5th of these residual phases. Extensive test runs have shown that taking every 5th screen is a good trade-off between computational needs and resulting accuracy. This is also in good agreement with the turbulence coherence time for the minimal turbulence scale of interest $\delta x = 0.125\ m$. Note that this temporal downsampling is done only for the computation of $\bar{D}_{\phi_\perp}$.

Note, that the c_n^2-profile used for the simulation is not changing and will in reality not perfectly match with the one during observation. OCTOPUS has a parameter called *turbulent_seed*, defining the starting point for the generation of atmospheric layers in a pseudo-random way. In order to avoid an unrealistic setting, we take different values of *turbulent_seed* for estimating $\bar{D}_{\phi_\perp}$ and the on-the-fly computation for estimating $D_{\phi_\parallel}$. In particular, this
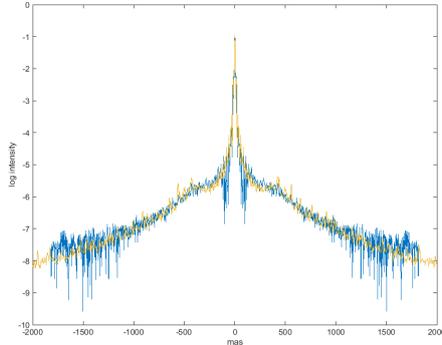
Figure 1: Comparison of the true PSF (yellow) and the reconstructed PSF (blue) for $n_{ph} = 1000$, cut through the main diagonal.

prevents that $\bar{D}_{\phi_\perp}$ and $D_{\phi_\parallel}$ match perfectly for the used atmosphere. However, using the same atmospheric profile still is a very optimistic approach.

4.3   Numerical results for high photon flux

We investigate the high flux case with $n_{ph} = 1000$, i.e., 1000 photons reach each subaperture in every time step in the setting of Table 1. In Figure 1, we compare (on a log-scale) cuts through the x-axis of the PSF reconstructed by our algorithm and the PSF calculated by ESO's OCTOPUS simulation tool. The latter one is a reference as it is calculated directly from the simulated atmosphere and averaged over time. However, both PSFs are in the plane of the WFS and not in the plane of the science image, but still at the science wavelength of 2.2 μm. This means that the simulation does not account for non common path errors of the system. Furthermore, also effects of the telescope, such as jitter, are not simulated.

In our simulations, we find a very good agreement between the reconstructed and the true PSF in the core. As our spatial resolution is limited, this translates into a limited coverage of the wings. However, we observe only little errors inside the DM control region. In order to provide a clearer view on the core of the PSF, we show a zoom in Figure 2 to highlight the differences between the reconstructed and the true PSF. From the PSF several parameters can be deduced, for example, the Strehl ratio. As the Strehl ratio relates the peaks of the seeing limited PSF and the diffraction limited PSF, dividing the peak of the reconstructed PSF by the peak of the true
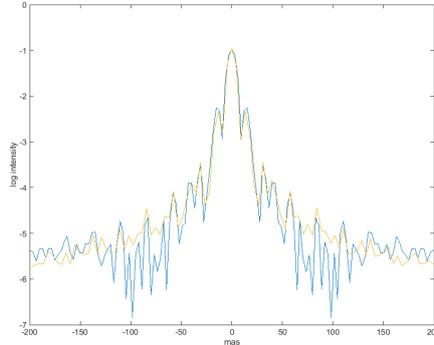
14

Figure 2: Zoom to the center of the true PSF (yellow) and the reconstructed PSF (blue) for $n_{ph} = 1000$, cut through the main diagonal.

PSF gives the accuracy of the Strehl ratio, i.e.,

$$\frac{|SR_{true} - SR_{rec}|}{SR_{true}},$$

where SR_{true} and SR_{rec} are the Strehl ratios calculated from the true and the reconstructed PSF, respectively. Note, that without particular tuning of the loop gain, the used AO control algorithm, CuReD [37, 31], reaches a Strehl ratio of 77.9%. In our computations, we find that the peak (and thus the Strehl ratio) is underestimated by only 0.4%, i.e., our reconstructed PSF suggests a Strehl ratio of only 77.6%.

Here, we do not present more parameters of the PSF for characterization as this work shall just demonstrate the feasibility of PSF reconstruction on ELTs and the science cases for the respective instruments are still under development. Therefore, also the metrics to be used are still not defined.

4.3.1 Influence of 2D and 4D structure function

In Section 3.1, we modified the PSF reconstruction for SCAO by using a 4D structure function $D_{\phi_{\parallel}}(x, \rho)$ instead of the 2D version used in Véran's algorithm. We now want to compare the effect of using these two different versions of the structure function. Clearly, the 4D version is computationally more demanding, but still can be computed in reasonable time on a modern computer.
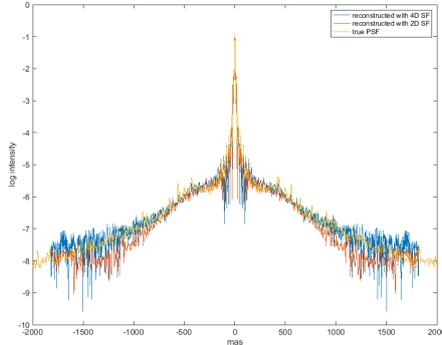
Figure 3: Comparison of the true PSF (yellow), the reconstructed PSF with a 2D structure function (red) and 4D structure function (blue) for $n_{ph} = 1000$, cut through the main diagonal.

The result when using the above high flux setting is shown in Figure 3. We found that the reconstruction of the PSF slightly improves when using the 4D structure function instead of the 2D. Comparing the Strehl ratios leads to an improvement from an error of 1% with the 2D structure function to an error of 0.4% error with the 4D structure function. Zooming into the center (see Figure 4) highlights another improvement in the first PSF ring, which is less overestimated using a 4D structure function. These results show that even if a 4D structure function can be computed and used for PSF reconstruction in realistic conditions, i.e., in the presence of noise and NCPAs, still a 2D structure function might be adequate. However, as long as the computation time for a 4D structure function is feasible, it will be our method of choice in order to avoid methodical errors.

4.4 Numerical results for low photon flux

In the previous subsections, we considered a fixed physical setup and varied some computational parameters. In real observations also the physical setup, mainly the photon flux coming from the guide star, will vary from one observation to another. In particular, certain observations will require the use of faint guide stars. Therefore, the proposed algorithm should give reliable results also for lower photon flux.

The telescope and simulation setup remains as in Table 1. For this section, we also test both versions, the 2D and the 4D structure function, for
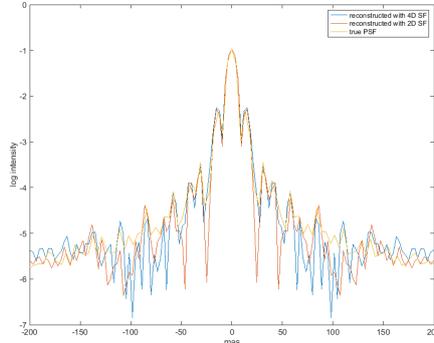
Figure 4: Zoom to the center of the comparison of the true PSF (yellow), the reconstructed PSF using a 2D structure function (red) and a 4D structure function (blue) for $n_{ph} = 1000$, cut through the main diagonal.

$\phi_{\parallel}$. Furthermore, the c_n^2-profile remains constant and therefore we can use the same $\bar{D}_{\phi_{\perp}}$ as in the previous section.

Figure 5 shows the reconstructed PSF and the true PSF for $n_{ph} = 500$. The Strehl ratio calculated from OCTOPUS is 77.4%. As in the high flux case, the difference between the true and the reconstructed PSF is small and the Strehl ratio is estimated very well. Using a 4D structure function the error in the Strehl ratio is again only 0.4% for the 4D version, and is thus in the same regime as for the high flux case. Using the 2D structure function gives a similar quality loss as in the high flux case and results in an error for the Strehl ratio of 1%.

Reducing the flux further to $n_{ph} = 100$ gives the results displayed in Figure 6 and a drop of the Strehl ratio to 73%. For our simulation setting, we obtain an error in Strehl ratio in the same regime as for higher photon flux, for both the 2D and 4D version of the structure function.

5 Conclusion and outlook

In this work, we presented an algorithm for PSF reconstruction in an SCAO system for the upcoming generation of ELTs. In contrast to Véran's algorithm, our approach is based on wavefronts rather than on measurements and uses the 4D structure function for the mirror modes, while sticking to a 2D
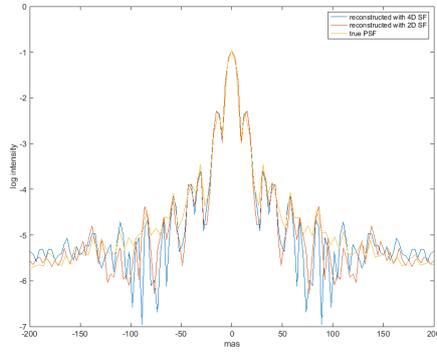
Figure 5: Zoom to the center of the comparison of the true PSF (yellow) and the reconstructed PSF with 4D structure function (blue) and 2D structure function (red) for $n_{ph} = 500$, cut through the main diagonal.
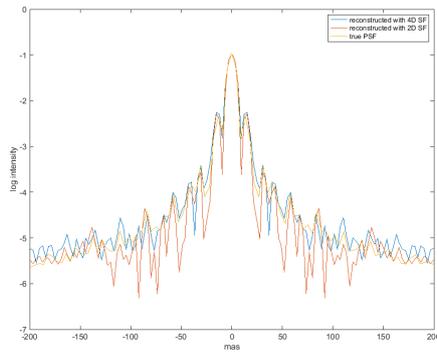

Figure 6: Zoom to the center of the comparison of the true PSF (yellow) and the reconstructed PSF with 4D structure function (blue) and 2D structure function (red) for $n_{ph} = 100$, cut through the main diagonal.

calculation for the perpendicular part. First simulations show qualitatively good reconstruction of the PSF compared to the PSF calculated directly from the simulated incoming wavefront. Furthermore, the used algorithm has a reasonable runtime and memory consumption.

The algorithm can be further improved by a more accurate model for the noise covariance used in $D_{\phi_\parallel}$.

Future goals, are to develop a version of the proposed algorithm which can be used for PSF reconstruction in a multi-conjugate adaptive optics (MCAO) system, where PSF knowledge across the whole field of view is required an can be obtained using measurements from all GS. Furthermore, we want to include the effects of anisoplanatism for off-axis PSF reconstruction into our algorithm.

Additionally, we want to use the reconstructed PSFs as input in a blind deconvolution algorithm for image improvement, which can be done after the observation on the telescope. Such an approach leads to a further improvement of the quality of the reconstructed PSF and simultaneously improves the quality of the observed image. First results for a simplified setting can be found, e.g., in [14].

As PSF reconstruction shall be performed on the ELT once it is operational, there are several steps to tackle before that. Once the hardware specifications are fixed, we want to further investigate the performance of the algorithm when using a faint guide star as well as with bad seeing conditions. The next steps will then be the incorporation to a bench before moving to an existing telescope. In order to complete these steps successfully, we need to incorporate residual NCPAs after internal correction into our algorithm. Furthermore, as for the ELT most likely the science target will be off-axis, our algorithm has to be extended to deal with anisoplanatism.

Acknowledgments

References

[1] D. S. Acton. Correction of static optical errors in a segmented adaptive optical system. *Appl. Opt.*, 34(34):7965–7968, Dec 1995.

[2] M. Aubailly, M. Roggemann, and T. Schulz. Approach for reconstructing anisoplanatic adaptive optics images. *Applied Optics*, 46(24):6055–6063, Aug 2007.

[3] N. Bharmal, U. Bitenc, A. Basden, R. Myers, and N. Dipper. A hierarchical wavefront reconstruction algorithm for gradient sensors. In *Third AO4ELT Conference – Adaptive Optics for Extremely Large Telescopes*, 2013.

[4] U. Bitenc, A. Basden, N. Ali Bharmal, T. Morris, N. Dipper, E. Gendron, F. Vidal, D. Gratadour, G. Rousset, and R. Myers. On-sky tests of the CuReD and HWR fast wavefront reconstruction algorithms with CANARY. *Monthly Notices of the Royal Astronomical Society*, 448(2):1199–1205, 2015.

[5] B. Brandl, T. Agócs, G. Aitink-Kroes, T. Bertram, F. Bettonvil, R. van Boekel, O. Boulade, M. Feldt, A. Glasse, A. Glauser, M. Güdel, N. Hurtado, R. Jaeger, M. Kenworthy, M. Mach, J. Meisner, M. Meyer, E. Pantin, S. Quanz, H. Schmid, R. Stuik, A. Veninga, and C. Waelkens. Status of the mid-infrared e-elt imager and spectrograph metis. In *Proceedings of the SPIE, Volume 9908*, page 990820, 2016.

[6] M.C. Britton. The anisoplanatic point spread function in adaptive optics. *Publications of the Astronomical Society of the Pacific*, 118(844):885–900, June 2006.

[7] R. Chan, X. Yuan, and W. Zhang. Point spread function reconstruction in ground-based astronomy by l1-lp model. *JOSA A*, 29:2263–2271, 2012.

[8] Y. Clénet, C. Lidman, E. Gendron, G. Rousset, T. Fusco, N. Kornweibel, M. Kasper, and N. Ageorges. Tests of the PSF reconstruction algorithm for NACO/VLT. In *Proc. SPIE 7015, Adaptive Optics Systems, 701529*, 2008.

[9] J.-M. Conan, L. Mugnier, T. Fusco, V. Michau, and G. Rousset. Myopic deconvolution of adaptive optics images by use of object and point-spread function power spectra. *Applied Optics*, 37(21):4614–4622, 1998.

[10] R. Davies and M. Kasper. Adaptive optics for Astronomy. *Annual Review of Astronomy and Astrophysics*, 50:305–351, 2012.

[11] R. Davies, J. Schubert, M. Hartl, J. Alves, Y. Clénet, F. Lang-Bardl, H. Nicklas, J.-U. Pott, R. Ragazzoni, E. Tolstoy, T. Agocs, H. Anwand-Heerwart, S. Barboza, P. Baudoz, R. Bender, P. Bizenberger, A. Boccaletti, W. Boland, P. Bonifacio, F. Briegel, T. Buey, F. Chapron, M. Cohen, O. Czoske, S. Dreizler, R. Falomo, P. Feautrier, N. Förster Schreiber, E. Gendron, R. Genzel, M. Glück, D. Gratadour, R. Greimel, F. Grupp, M. Häuser, M. Haug, J. Hennawi, H. J. Hess, V. Hörmann, R. Hofferbert, U. Hopp, Z. Hubert, D. Ives, W. Kausch, F. Kerber, H. Kravcar, K. Kuijken, M. Leitzinger, K. Leschinski, D. Massari, S. Mei, F. Merlin, L. Mohr, A. Monna, F. Müller, R. Navarro, M. Plattner, N. Przybilla, R. Ramlau, S. Ramsay, T. Ratzka, P. Rhode, J. Richter, H.-W. Rix, G. Rodeghiero, R.-R. Rohloff, G. Rousset, R. Ruddenklau, V. Schaffenroth, J. Schlichter, A. Sevin, R. Stuik, E. Sturm, J. Thomas, N. Tromp, M. Turatto, G. Verdoes-Kleijn, F. Vidal, R. Wagner, M. Wegner, W. Zeilinger, B. Ziegler, and G. Zins. MICADO: first light imager for the E-ELT. In *Proc. SPIE 9908, Ground-based and Airborne Instrumentation for Astronomy VI*, volume 1, page 99081Z, 2016.

[12] L. Denis, E Thiébaut, and F. Soulez. Fast model of space-variant blurring and its application to deconvolution in astronomy. In *ICIP*, pages 2873–2876, 2011.

[13] G. Desiderà and M. Carbillet. Strehl-constrained iterative blind deconvolution for post-adaptive-optics data. *Astronomy & Astrophysics*, 507:1759–1762, 2009.

[14] L. Dykes, R. Ramlau, L. Reichel, K.M. Soodhalter, and R. Wagner. Lanczos-based fast blind deconvolution methods. *RICAM Report*, 2017-27, 2017.

[15] ESO. The European Extremely Large Telescope Project - Website. https://www.eso.org/sci/facilities/eelt/, 2018.

[16] J. Exposito, D. Gratadour, G. Rousset, Y. Clénet, E. Gendron, and L. Mugnier. A new method for adaptive optics point spread function reconstruction. In *Third AO4ELT Conference – Adaptive Optics for Extremely Large Telescopes*, May 2013.

[17] R.C. Flicker. PSF reconstruction for keck AO: Phase 1 final report. *W.M. Keck Observatory, 65-1120 Mamalahoa Hwy., Kamuela, HI 96743, USA*, 2008.

[18] D. Fried. Anisolplanatism in adaptive optics. *J. Opt. Soc. Am.*, 72(1):52–61, 1982.

[19] E. Gendron, Y.Clénet, T.Fusco, and G. Rousset. New algorithms for adaptive optics point-spread function reconstruction. *Astronomy & Astrophysics*, 457(1):359–463, Oct 2006.

[20] L. Gilles, C. Correia, J.-P. Véran, L. Wang, and B. Ellerbroek. Simulation model based approach for long exposure atmospheric point spread function reconstruction for laser guide star multiconjugate adaptive optics. *Applied Optics*, 51(31):7443–7458, Nov 2012.

[21] C. Hofer. Point spread function reconstruction for singleconjugated adaptive optics systems. Master's thesis, Johannes Kepler University Linz, 2014.

[22] L. Jolissaint, J. Christou, P. Wizinowich, and E. Tolstoy. Adaptive optics point spread function reconstruction: lessons learned from on-sky experiment on Altair/Gemini and pathway for future systems. In *Proc. SPIE 7736, Adaptive Optics Systems II, 77361F*, 2010.

[23] L. Jolissaint, C. Neyman, J. Christou, P. Wizinowich, and L. Mugnier. First Successful Adaptive Optics PSF Reconstruction at W. M. Keck Observatory. In *Proc. SPIE 8447, Adaptive Optics Systems III, 844728*, 2012.

[24] M. LeLouarn. Private communication.

[25] O. A. Martin, C. M. Correia, E. Gendron, G. Rousset, D. Gratadour, F. Vidal, T. J. Morris, A. G. Basden, R. M. Myers, B. Neichel, and T. Fusco. PSF reconstruction validated using on-sky CANARY data in MOAO mode. In *Proc. SPIE 9909, Adaptive Optics Systems V*, 2016.

[26] J. Nagy, S. Jefferies, and Q.Chu. Fast PSF reconstruction using the frozen flow hypothesis. In *Proceedings of the Advanced Maui Optical and Space Surveillance Technologies Conference*, 2010.

[27] A. Neubauer. A new cumulative wavefront reconstructor for the Shack-Hartmann sensor. *J. Inv. Ill-Posed Problems*, 21:451–476, 2013.

[28] M. Prato, A. La Camera, S. Bonettini, and M. Bertero. A convergent blind devoncolution method for post-adaptive-optics astronomical imaging. *Inverse Problems*, 29:065017, 2013.

[29] S. Ragland, L. Jolissaint, P. Wizinowich, M.A. van Dam, L. Mugnier, A. Bouxin, J. Chock, S. Kwok, J. Mader, G. Witzel, Tuan Do, M. Fitzgerald, A. Ghez, J. Lu, G. Martinez, , M.R. Morris, and B. Sitarski. Point spread function determination for keck adaptive optics. In *Proc. SPIE 9909, Adaptive Optics Systems V*, 2016.

[30] R. Rampy, S. Ragland, P. Wizinowich, and R. Campbell. Understanding and correcting low order residual static aberrations in adaptive optics corrected images. volume 9148, pages 9148 – 9148 – 17, 2014.

[31] M. Rosensteiner. Cumulative reconstructor: fast wavefront reconstruction algorithm for Extremely Large Telescopes. *J. Opt. Soc. Am. A*, 28(10):2132–2138, Oct 2011.

[32] M. Rosensteiner. Wavefront reconstruction for extremely large telescopes via CuRe with domain decomposition. *J. Opt. Soc. Am. A*, 29(11):2328–2336, Nov 2012.

[33] Pietro Schipani, Lothar Noethe, Carmelo Arcidiacono, Javier Argomedo, Massimo Dall'Ora, Sergio D'Orsi, Jacopo Farinato, Demetrio Magrin, Laurent Marty, Roberto Ragazzoni, and Gabriele Umbriaco. Removing static aberrations from the active optics system of a wide-field telescope. *J. Opt. Soc. Am. A*, 29(7):1359–1366, Jul 2012.

[34] J.-P. Véran, F. Rigaut, H. Maître, and D. Rouan. Estimation of the adaptive optics long exposure point spread function using control loop data. *J. Opt. Soc. Am. A*, 14(11):3057–3069, Nov 1997.

[35] R. Wagner. *From Adaptive Optics systems to Point Spread Function Reconstruction and Blind Deconvolution for Extremely Large Telescopes.* PhD thesis, Johannes Kepler University Linz, 2017.

[36] R. Wagner, A. Neubauer, and R. Ramlau. Simulation results for a finite element-based cumulative reconstructor. *Journal of Astronomical Telescopes, Instruments, and Systems*, 3(4):049001, 2017.

[37] M. Zhariy, A. Neubauer, M. Rosensteiner, and R. Ramlau. Cumulative wavefront reconstructor for the Shack-Hartman sensor. *Inverse Problems and Imaging*, 5(4):893–913, Nov 2011.